Experimental investigation of acoustically enhanced colloid transport in water-saturated packed columns

ARTICLE *in* JOURNAL OF COLLOID AND INTERFACE SCIENCE · MAY 2007

Impact Factor: 3.55 · DOI: 10.1016/j.jcis.2006.12.062 · Source: PubMed

2 AUTHORS, INCLUDING:

Constantinos V. Chrysikopoulos
Technical University of Crete
143 PUBLICATIONS **1,994** CITATIONS

Available online at www.sciencedirect.com
ScienceDirect
Journal of Colloid and Interface Science 308 (2007) 200–207
JOURNAL OF Colloid and Interface Science
www.elsevier.com/locate/jcis

Experimental investigation of acoustically enhanced colloid transport in water-saturated packed columns

J. Matthew Thomas [a,*], Constantinos V. Chrysikopoulos [b]

[a] *Department of Civil and Environmental Engineering, University of California, Irvine, CA 92697, USA*
[b] *Department of Civil Engineering, University of Patras, Patras 26500, Greece*

Received 28 September 2006; accepted 21 December 2006

Available online 28 December 2006

Abstract

The effects of acoustic wave propagation on the transport of colloids in saturated porous media were investigated by injecting Uranine (conservative tracer) as well as blue and red polystyrene microspheres (colloids of different diameters; 0.10 and 0.028 μm, respectively) into a column packed with glass beads. Experiments were conducted by maintaining the acoustic pressure at the influent at 23.0 kPa with acoustic frequencies ranging from 30 to 150 Hz. The experimental results suggested that colloid size did not affect the forward and reverse attachment rate coefficients. The acoustic pressure caused an increase in the effective interstitial velocity at all frequencies for the conservative tracer and colloids of both sizes, with maximum increase at 30 Hz. Furthermore, acoustics enhanced the dispersion process at all frequencies, with a maximum at 30 Hz.

Keywords: Colloid transport; Acoustic waves; Enhanced transport; Subsurface transport; Polystyrene microspheres

1. Introduction

Groundwater aquifers are often contaminated by an assortment of pollutants that derive from various sources. One common class of groundwater contaminants is dissolved molecular solutes. Examples include pesticides and fertilizers from agricultural runoff, nitrate and nitrite from wastewater release, and radionuclides that can leach into groundwater from deep geological disposal sites. Another common class of groundwater pollutants is colloidal particles such as viruses and bacteria (biocolloids) from domestic or industrial wastewater spills. A third common class of pollutant is dissolved light or dense non-aqueous phase liquids (DNAPLs) such as TCE, PCE, and gasoline by-products from leaking storage tanks, leaking pipelines, or accidental spills [1–4]. In addition, natural colloidal particles (very fine particles that have some linear dimension between 0.001 and 10 μm [5]) are ubiquitous in groundwater aquifers, and may significantly affect the subsurface fate and transport of these contaminants.

Typical colloids present in groundwater include clay minerals, oxides or hydroxides of Fe and Al, colloidal silica, and organic matter such as humic macromolecules [6–10]. The large specific surface areas of these colloids cause relatively weak forces such as van der Waals forces, electric double layer forces, and electrostatic forces to have a profound effect on their transport and deposition. Experimental evidence has shown that colloids can have a faster breakthrough compared to solute tracers in packed columns (e.g., [9,11–14]). This effect is attributed to size exclusion and electrostatic repulsive forces [15]. It is also widely accepted that colloids migrate faster than nonsorbing conservative tracers in natural fractures [16–18]. Enhanced mobility of colloids in porous media depends on the size of the pore spaces and on the nature of the colloid–matrix interactions (surface chemistry). Unfavorable deposition interactions result in enhanced mobility [17].

There is also substantial evidence from both laboratory and field experiments that colloids are efficient sorbents for contaminants such as heavy metals, nonpolar organic compounds, and radionuclides [15,19,20]. Tatalovich et al. [10] showed that applying humic substances to groundwater contaminated with a DNAPL pool enhanced the mass transfer of DNAPL to the

* Corresponding author. Fax: +1 949 297 4156.
E-mail address: jmthomas@uci.edu (J.M. Thomas).

0021-9797/$ – see front matter
doi:10.1016/j.jcis.2006.12.062

aqueous phase. Parametric investigations have also shown that liquid-phase contaminant concentration of DNAPL is sensitive to the partition coefficient for contaminant sorption onto suspended colloids [16]. The ability of contaminants to adsorb onto colloids and of colloids to experience enhanced mobility (colloid-associated transport) may contribute to faster contaminant migration and dispersion, which exacerbates the contamination problem.

In many parts of the world, including the United States, groundwater is often pumped and distributed directly into homes for consumption without any processing. Consequently, the prevalence, toxicity, and mobility of contaminants has facilitated interest in groundwater remediation techniques. There are a number of available technologies for treatment of contaminated groundwater that have been utilized with varying degrees of success: filtration through granular activated carbon (GAC), soil removal and/or washing, air stripping, and biological contact or trickle filtration. These remediation technologies rely heavily on pump-and-treat methodologies such that the amount of contaminant mass removed is proportional to the amount of water pumped from the subsurface and to the concentration of dissolved or suspended contaminant in that water. Therefore, groundwater remediation is limited by the aqueous solubility of the particular contaminant. Unfortunately, several of the contaminants present in groundwater have low aqueous solubilities (e.g., DNAPLs [21]), or high affinities for adsorption onto the subsurface formation creating a long persisting source of contamination. Various methods have been explored in recent years to enhance contaminant transport and dissolution to address this issue. Some methods involve introduction of nonindigenous colloids or humic substances, specialized biocolloids, surfactants, or cosolvents. These methods could be problematic as all of the added substances are considered to be either contaminants themselves or undesirable in the drinking water supply.

A desired groundwater remediation approach is a 'clean' technology that will increase contaminant mass transport and dissolution in porous media with conventional pump-and-treat methods, thereby facilitating enhanced remediation without adding further contaminants to the subsurface. An example of such a technology is the introduction of acoustic (sound) waves in saturated porous media to increase contaminant mass transport. Building on the fundamental work of Biot [22,23], the theory of acoustic propagation in porous media has been studied extensively in soil mechanics, seismology, earthquake engineering, geophysics, and petroleum engineering [24]. However, only recently has the concept of using waves for aquifer remediation been given attention and several preliminary studies have been conducted. For example, acoustic waves were found to enhance transport of a conservative tracer in packed column experiments with the effective velocity of the solute being approximately inversely proportional to the frequency of the acoustic wave [25]. Other theoretical and experimental results have shown that significant displacement of solutes in saturated porous media results from the propagation of different types of compression waves (e.g., compaction waves and short and long shock waves), even in the absence of background flow [1]. Experimental evidence also shows that acoustic waves can increase both mobilization and dissolution in multi-phase systems (i.e., NAPL/water) [24,26–28]. Thomas and Narayanan [29] showed that solute mass transfer is enhanced by several orders of magnitude when the fluid medium is subject to oscillatory motion, even if there is no net total flow over a cycle of oscillation. Experimental evidence has shown that effluent aqueous DNAPL concentration increased with the application of acoustic pressure waves with the greatest dissolution enhancement occurring at lower frequencies [26]. Furthermore, ganglia that were immobile under steady background flow were mobilized when acoustic pressure was added [27,28]. Gross et al. [1] have suggested that the unique significance and economic potential of introducing pressure waves into an aquifer is in the ability to focus on cleaning groundwater at localized sites, mobilize trapped contaminants, and guide the motion of a contaminant plume by controlling the intensity and direction of the applied pressure. However, the effects of acoustic waves on colloid transport in saturated porous media have not been investigated, and they are the focus of the present work.

Whether colloids present in groundwater are contaminants themselves, natural colloids that facilitate contaminant transport, or nonindigenous colloids used for remediation, understanding the effects of acoustic wave application on the transport of colloids in saturated porous media is necessary before acoustics can be applied for aquifer remediation.

2. Mathematical model development

The one-dimensional advection–dispersion equation for colloidal particles in homogeneous saturated porous media accounting for adsorption (or filtration) and inactivation under a constant hydraulic gradient is given by the following linear second-order partial differential equation:

$$\frac{\partial C(t,x)}{\partial t} + \frac{\rho}{\theta}\frac{\partial C^*(t,x)}{\partial t} = D_e\frac{\partial^2 C(t,x)}{\partial x^2} - U_e\frac{\partial C(t,x)}{\partial x} - \lambda C(t,x) - \lambda^*\frac{\rho}{\theta}C^*(t,x), \quad (1)$$

where C is the concentration of colloids in suspension [M/L^3], C^* is the mass of colloids adsorbed on the porous medium [M/M], D_e is the effective hydrodynamic dispersion coefficient [L^2/t], U_e is the effective interstitial fluid velocity [L/t], ρ is the bulk density of the porous medium [M/L^3], λ is the inactivation constant of suspended colloids [t^{-1}], λ^* is the inactivation constant of adsorbed colloids [t^{-1}], θ is the porosity of the porous medium [–], and t is time [t]. Inactivation was included in the governing transport equation so that the solution can be applied to biocolloids and radiocolloids, though they were not studied in the present work. The effective interstitial fluid velocity is defined as [25]

$$U_e = U + U^*, \quad (2)$$

where U is the steady-state background interstitial fluid velocity [L/t], and U^* is the additional velocity component attributed to acoustic pressure [L/t]. Similarly, the effective dispersion coefficient is defined as

$$D_e = D + D^* = (U + U^*)\alpha_L + \mathcal{D}_e = U_e\alpha_L + \mathcal{D}_e, \quad (3)$$

where $D = U\alpha_L + \mathcal{D}_e$ is the hydrodynamic dispersion coefficient [L^2/t], α_L is the longitudinal dispersivity [L], $\mathcal{D}_e = \mathcal{D}/\tau^*$ is the effective molecular diffusion coefficient [L^2/t] (where $\mathcal{D}$ is the molecular diffusion coefficient [L^2/t], and $\tau^* > 1$ is the tortuosity coefficient [–]), and D^* is the additional dispersion component attributed to acoustic pressure [L^2/t]. It should be noted that the concept of effective parameters has been applied in numerous groundwater flow and solute transport studies [25,30–34]. The rate of colloid attachment onto the solid matrix is described by the following first-order equation [35]:

$$\frac{\rho}{\theta}\frac{\partial C^*(t,x)}{\partial t} = r_1 C(t,x) - r_2 C^*(t,x) - \lambda^*\frac{\rho}{\theta}C^*(t,x), \tag{4}$$

where r_1 is the forward attachment rate coefficient [t^{-1}], and r_2 is the reverse attachment rate coefficient [$M/L^3/t$].

The desired expression for C^* is obtained by solving (4) subject to an initial condition of zero sorbed (or filtered) colloid concentration ($C^*(0,x) = 0$) as

$$C^*(t,x) = \frac{r_1\theta}{\rho}\int_0^t C(\tau,x)\exp\left[-\left(\frac{r_2\theta}{\rho}+\lambda^*\right)(t-\tau)\right]d\tau. \tag{5}$$

In view of (2)–(5) the governing equation (1) can be written as

$$\frac{\partial C(t,x)}{\partial t} = D_e\frac{\partial^2 C(t,x)}{\partial x^2} - U_e\frac{\partial C(t,x)}{\partial x} - \mathcal{A}C(t,x) + \mathcal{B}\int_0^t C(\tau,x)\exp\big[-\mathcal{H}(t-\tau)\big]d\tau, \tag{6}$$

where the following substitutions have been employed:

$$\mathcal{A} = r_1 + \lambda, \tag{7}$$

$$\mathcal{B} = \frac{r_1 r_2\theta}{\rho}, \tag{8}$$

$$\mathcal{H} = \frac{r_2\theta}{\rho} + \lambda^*. \tag{9}$$

For a semi-infinite one-dimensional porous medium, the appropriate initial and boundary conditions are given by

$$C(0,x) = 0, \tag{10}$$

$$-D_e\frac{\partial C(t,0)}{\partial x} + U_e C(t,0) = M_0\delta(t), \tag{11}$$

$$\frac{\partial C(t,\infty)}{\partial x} = 0, \tag{12}$$

where $M_0 = M_I/A\theta$ is the mass injected over the cross-sectional area of the column (where M_I is the injected mass [M] and A is the cross sectional area of the porous medium [L^2]), and δ is the Dirac delta function [t^{-1}]. Initial condition (10) establishes a zero background colloid concentration. Boundary condition (11) describes the flux influent pulse concentration. The downstream boundary condition (12) preserves concentration continuity for a semi-infinite system. The solution to the governing equation (6) subject to conditions (10)–(12) is obtained analytically by Laplace transform and inverse Laplace transform techniques following the methods of Lapidus and Amundson [36], Chrysikopoulos et al. [31], and Sim and Chrysikopoulos [35,37,38]:

$$\begin{aligned} C(t,x) = {} & \frac{M_0}{\sqrt{D_e}}\exp\left[\frac{U_e x}{2D_e} - \mathcal{H}t\right] \\ & \times\left\{\frac{\exp\left[\frac{-x^2}{4D_e t} + \left(\mathcal{H} - \mathcal{A} - \frac{U_e^2}{4D_e}\right)t\right]}{\sqrt{\pi t}}\right. \\ & - \frac{U_e}{2\sqrt{D_e}}\exp\left[\frac{U_e x}{2D_e} + (\mathcal{H}-\mathcal{A})t\right] \\ & \times \operatorname{erfc}\left[\frac{x}{2\sqrt{D_e t}} + \frac{U_e}{2}\sqrt{\frac{t}{D_e}}\right] \\ & + \int_0^t \frac{\mathcal{B}\zeta}{\sqrt{\mathcal{B}\zeta(t-\zeta)}} I_1\left[2\sqrt{\mathcal{B}\zeta(t-\zeta)}\right] \\ & \times\left[\frac{\exp\left[\frac{-x^2}{4D_e\zeta} + \left(\mathcal{H} - \mathcal{A} - \frac{U_e^2}{4D_e}\right)\zeta\right]}{\sqrt{\pi\zeta}}\right. \\ & - \frac{U_e}{2\sqrt{D_e}}\exp\left[\frac{U_e x}{2D_e} + (\mathcal{H}-\mathcal{A})\zeta\right] \\ & \left.\left.\times \operatorname{erfc}\left[\frac{x}{2\sqrt{D_e\zeta}} + \frac{U_e}{2}\sqrt{\frac{\zeta}{D_e}}\right]\right]d\zeta\right\}, \end{aligned} \tag{13}$$

where 'exp' is the exponential function, 'erfc' is the complementary error function, I_1 is the modified Bessel function of order one, and ζ is a dummy integration variable.

3. Experimental design and procedures

3.1. Experimental apparatus

The effects of acoustic wave propagation on colloid transport through saturated porous media were investigated by injecting a multi-component (colloids and molecular solute) tracer pulse into a 30 cm long CHROMAFLEX glass column with a 2.5 cm inner diameter (Kimble Kontes, New Jersey). The column was packed with 2 mm diameter soda-lime glass beads (Fisher Scientific, New Jersey). Glass beads were chosen as model porous media because they are chemically non-reactive with the solutions used in this study. The beads were retained in the column with high density polyethylene (HDPE) screens, which were held in place by polytetrafluoroethylene (PTFE) (Teflon) column end fittings on both the influent and effluent ends. The end fittings were milled to accommodate 1/4 inch stainless steel fittings (Swageloc) for 3/8 inch semi-rigid plastic tubing (Fisher Scientific, Pennsylvania). This bore allowed unimpeded water flow and acoustic wave propagation from the reservoir through the column. The end fittings were secured by plastic screw caps that screw into threads molded in the ends of the glass column. HDPE, PTFE, and stainless steel are chemically non-reactive with the solutions and colloids used. Constant flow of purified water at a rate of 0.80 ml/min was maintained through the packed column with a dual-syringe infusion pump (KDS200; KD Scientific, Massachusetts). Use of a syringe injector ensured consistent tracer injections between experiments. Acoustic pressure waves were introduced into the column by

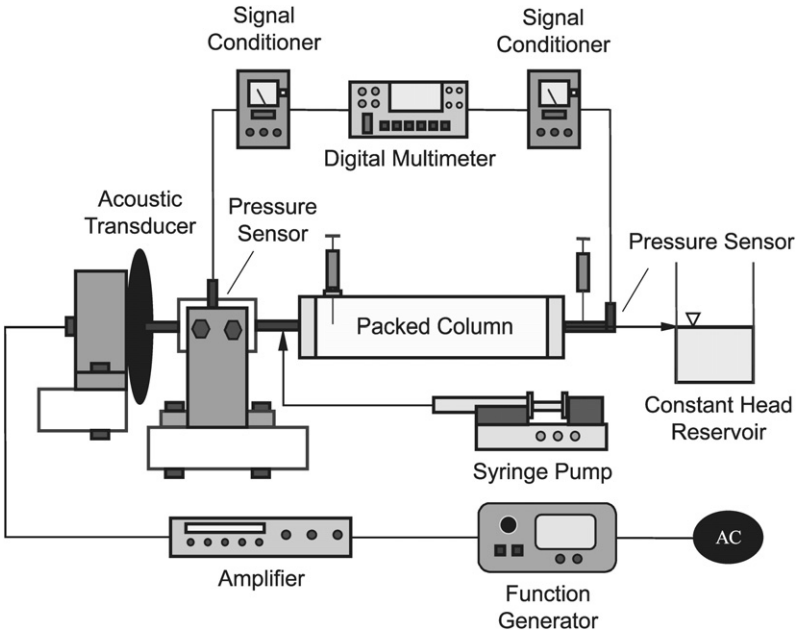

Fig. 1. Experimental apparatus.

the oscillation of a tactile sound transducer (TST429; Clark Synthesis, Colorado), that was mounted securely to a separate laboratory countertop to limit vibration so that all the acoustic energy would be transferred to the column. A small plunger was connected to the transducer on one end and fused to a neoprene diaphragm on the other end. The diaphragm was secured to a specially designed reservoir milled from a block of Plexiglas. The frequency of acoustic pressure oscillation was controlled by a function generator (FG-7002C; LG Precision, California) with a frequency setting accuracy of ±5% in the 10–1000 Hz range employed. The magnitude of acoustic pressure was controlled by an amplifier (Lab300; Lab Gruppen, Sweden) and was measured with PCB106b pressure sensors with a resolution of 0.00069 kPa and calibrated linearity ⩽1% (FS) in conjunction with 480E09 ICP sensor signal conditioners (PCB Piezotronics, Inc., New York) and a digital multimeter (MXD-4660A; Metex, Korea) with an accuracy of ±0.05000% in the 2V DC range employed. The pressure sensors were mounted on the influent and effluent ends of the glass-bead pack. Effluent samples were collected from a dedicated needle (sampling port) mounted with its sharpened end resting against the HDPE screen that retained the glass-bead pack on the effluent end of the column. A complete schematic of the experimental apparatus employed in this study is shown in Fig. 1.

3.2. Solution preparation

Experimental evidence suggests that both pH and ionic strength of the background solution significantly affect colloid transport and deposition [15]. Therefore, water used in these experiments was purified to a specific resistance of 18.2 mΩ cm with a Milli-Q UV plus water purification system (Millipore Corp., Massachusetts) containing a filter with 0.22 μm pore size and UV sterilization. The water was then vacuum degassed in a clean vacuum flask for at least 15 min to remove dissolved gases. Water was stored under vacuum to prevent absorption of carbon dioxide (CO_2) gas that would cause pH to fluctuate and affect colloid surface charges. Water throughout all experiments was maintained at pH 7.2. Stock solutions of the tracers employed were prepared. The conservative tracer stock solution was a 5 mg/L solution of Fluorescein Sodium Salt ($C_{20}H_{10}Na_2O_5$) commonly known as Uranine (Fisher Scientific, New Jersey). The blue microsphere (with diameter 0.10 μm and coefficient of variation (CV) <10%) and red microsphere (with diameter 0.028 μm and CV <20%) stock solutions were one-in-twenty dilutions of commercially available one-percent-by-mass solutions of fluorescent-dyed polystyrene microspheres (Duke Scientific, California). The colors (i.e., blue and red) correspond to the wavelengths of light of the emission spectrum of the fluorescent dye incorporated into the polystyrene matrix of the microspheres. The multi-component tracer injected into the column was made prior to each experiment by combining exactly 1.0 ml of a conservative tracer stock solution, 1.0 ml of blue microsphere stock solution, and 1.0 ml of red microsphere stock solution. Five dilutions of known concentration were made for quantification.

3.3. Experimental procedure

The base case experiment was first conducted to determine effluent concentrations for Uranine (conservative tracer) and the two different-sized microsphere suspensions (colloids) in the absence of acoustic waves (0 Hz) using the following procedure. A slug of 0.6 ml of the multi-component tracer solution was instantaneously injected with the syringe injector into the column through the injection port located near the influent end of the column. Elapsed time was measured with a digital quartz chronograph (Timex, New Jersey), and the temperature of the water was maintained throughout the experiments at 21 °C. Sample effluent volumes of 0.5 ml were collected from the

sampling port at regular two-minute intervals using a dedicated disposable 1.0 ml tuburculin plastic syringe (Becton Dickinson and Co., New Jersey). The samples were then transferred to 1 cm pathlength disposable polyethylene cuvettes (Cole Parmer Instrument Co., Illinois), where exactly 1.5 ml of Millipore-purified water was added using an eppendorf reference pipette (Brinkmann Instruments, Inc., New York). This dilution was necessary because the luminescence spectrometer used to analyze the samples requires a minimum sample volume of 2 ml. The sample cuvettes were then sealed with plastic cuvette lids (Fisher Scientific, New Jersey). Subsequent experiments were conducted using the same procedure described for the base case, but in the presence of acoustic waves at seven different preselected acoustic frequencies (30, 50, 70, 90, 110, 130, and 150 Hz). Column apparatus and all accessories were carefully cleaned between experiments by pumping several pore volumes of a strong acid (HCl) followed by several pore volumes of purified degassed water, similar to the process performed by Weronski et al. [39]. This procedure ensured that the column and media were free from contaminants and microorganisms and that solution chemistry was uniform between experiments. For all frequencies, acoustic pressure in the influent was set to 3.33 psi (23.0 kPa). Due to different attenuation of acoustic waves at different frequencies, the acoustic pressure in the effluent was different for each experimental frequency. The measured effluent acoustic pressures were 15.0, 15.7, 16.5, 16.9, 17.9, 19.7, and 20.2 kPa, respectively for the frequencies above. Influent and effluent pressures remained constant throughout each experiment.

3.4. Analysis

The effluent samples from the column which contained different concentrations of the three tracers were analyzed by performing emission scans with an Aminco-Bowman series 2 luminescence spectrometer (Thermo Spectronic, New York). The Uranine and microsphere suspensions were chosen because they exhibit fluorescent properties at different excitation wavelengths. Each effluent sample was excited three times; once at each excitation wavelength (412, 463, and 542 nm specific to blue microspheres, Uranine, and red microspheres, respectively). The emission wavelength ranges were carefully chosen to allow maximum fluorescence while minimizing any overlapping areas of the emission spectra. In this way the concentration of each species in a single effluent sample was determined independently.

Before the analytical solution (13) could be employed to fit the experimental breakthrough data, the parameters θ, ρ, and U associated with the column and glass beads were obtained. It should be noted that the variables $\mathcal{H}$ and U_e in Eq. (13) are functions of the parameters θ, ρ, and U. The porosity of the solid matrix (beads) is given by

$$\theta = \frac{V_v}{V_t} = \frac{V_t - V_b}{V_t}, \tag{14}$$

where V_v is the volume of the void space inside the packed column [L^3]; V_t is the total inner volume of the glass column [L^3], and V_b is the volume of the glass beads themselves in the column [L^3]. The total volume was calculated from the inner diameter and length of the column. The volume of the beads in the column was determined by transferring the beads to a graduated cylinder filled with water and measuring the volume of water they displaced. The bulk density is given by

$$\rho = \frac{M_b}{V_t}, \tag{15}$$

where M_b is the mass of the beads [M]. The average interstitial velocity is given by

$$U = \frac{q}{\theta} = \frac{Q}{A\theta}, \tag{16}$$

where q is the seepage or Darcy velocity [L/t] and Q is the volumetric flow rate [L^3/t]. The volumetric flow rate was set at 0.80 ml/min for all experiments and the cross-sectional area was calculated from the inner diameter of the column. The model parameter values are listed in Table 1.

Table 1
Column parameters

Parameter	Symbol	Value
Porosity	θ	0.368 [–]
Bulk density	ρ	1.60 [g/cm^3]
Average interstitial velocity	U	26.57 [cm/h]
Volumetric flow rate	Q	0.80 [ml/min]
Column length	–	30 [cm]
Inside diameter	–	2.5 [cm]

Subsequently, the Levenberg-Marquardt nonlinear least squares regression method was used with the analytical solution (13) to determine the effective dispersion coefficient and the effective velocity associated with each acoustic frequency. The objective of the nonlinear least squares method is to obtain estimates of the model parameters that minimize the sum of squared residuals between simulated and observed data. A FORTRAN program was written utilizing the subroutine mrqmin [40] for fitting the data and the subroutine qdag [41] for numerical evaluation of the integral present in Eq. (13).

4. Results and discussion

The experimental breakthrough data for Uranine in the absence of acoustic waves (base case) was fit to obtain $U = 26.56$ cm/h and $D = 5.40$ cm^2/h (see Eqs. (2) and (3)). Note that r_1 and r_2 are zero for conservative tracers such as Uranine. Since the effective molecular diffusion, $\mathcal{D}_e$, of Uranine is several orders of magnitude smaller than $U_e\alpha_L$, and is therefore negligible, the value of the longitudinal dispersivity, $\alpha_L = 0.203$ cm, was obtained from Eq. (3). Next, the experimental data for blue and red microspheres for the base case were fit for D, r_1, and r_2 using the interstitial velocity obtained from Uranine. The hydrodynamic dispersion coefficients for blue and red microspheres were 7.41 and 7.20 cm^2/h, respectively. The fitted values of r_1 and r_2 for blue and red microspheres were 0.136 and 61.6 h^{-1}; and 0.118 and 40.3 h^{-1}, respectively. For the low velocity used in these experiments, the small deposition rates

obtained agree with the work of Kretzschmar and Sticher [9], who have suggested a direct relationship between deposition rates and pore velocity. Although the dispersivity is a property of the porous medium, experimental evidence has shown that colloids experience a different dispersivity than conservative tracers in the same medium [14]. Longitudinal dispersivities were calculated from base case blue and red microsphere data as 0.279 and 0.271 cm, respectively. Subsequently, the values of U_e (for Uranine), and U_e, r_1, and r_2 (for colloids) were obtained for each frequency of acoustic pressure with the proper D_e being determined from Eq. (3) and the calculated dispersivities. Finally, the components of interstitial velocity and hydrodynamic dispersion attributed to acoustics, U^* and D^*, were obtained from Eqs. (2) and (3) with the base case values of U and D.

Fig. 2 shows the base case experimental data for Uranine and the two colloids together with the corresponding breakthrough curves fitted by the analytical solution (13). It can be seen that the analytical solutions match the experimental data well. The blue and red microspheres have a lower peak concentration and they exhibit more tailing at later times than Uranine, indicating that the colloids are adsorbing to and desorbing from the porous medium. The colloids experienced a slightly faster breakthrough time over the conservative tracer, as indicated by their higher concentrations at early times. Although early breakthrough due to size exclusion has been observed in various studies [14,16], very minor differences between blue and red microspheres were observed because the pore space created by 2 mm glass beads is quite large compared to the colloid diameters.

Fig. 3 shows experimental data and fitted breakthrough curves of the effluent blue microsphere concentrations for 0 (base case), 50, and 150 Hz acoustic oscillation frequency. Note that in the presence of acoustic waves, the breakthrough curves are shifted to the left, indicating an increased velocity, and spread more in the longitudinal direction, indicating an increased dispersion over the base case. Similar effects were observed for Uranine and the red microspheres with breakthrough curves for both colloids being nearly identical.

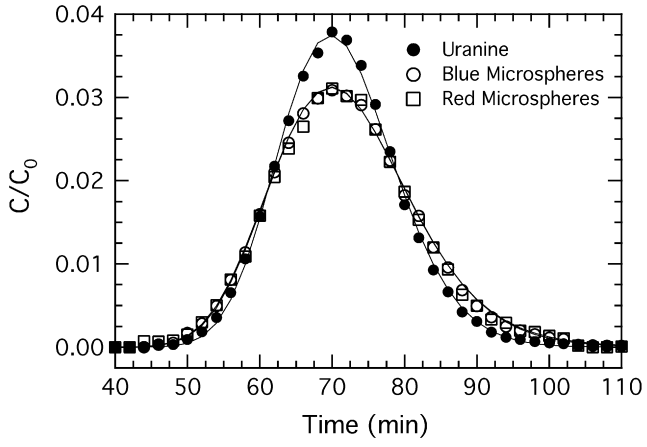

Fig. 2. Breakthrough data (symbols) and fitted analytical solutions (solid lines) for Uranine (solid circles), blue microspheres (open circles), and red microspheres (open squares), in the absence of acoustic waves (base case).

Fig. 4 displays the values of U^*, the additional component of interstitial velocity attributed to acoustics, determined from experiments at all frequencies employed for Uranine as well as blue and red microspheres. Both colloids were affected by acoustic waves in a similar fashion with slightly larger increased interstitial velocity than Uranine. Applied acoustic waves caused an increase in effective interstitial velocity at all frequencies employed for Uranine and both colloids. The most notable increase occurred at 30 Hz, where both colloids experienced the greatest increase in effective interstitial velocity. At 30 Hz, a relatively large volume of water must be oscillated by the transducer to generate the constant influent pressure (23.0 kPa) maintained in this study. This large oscillation was only observed at the lowest frequency in this study (30 Hz). The peak in U^* and consequently D^* at 30 Hz is attributed to this oscillating volume of water, though the exact mechanism must be studied further.

Fig. 5 displays the values of D^* determined from experiments at all frequencies employed for Uranine as well as blue

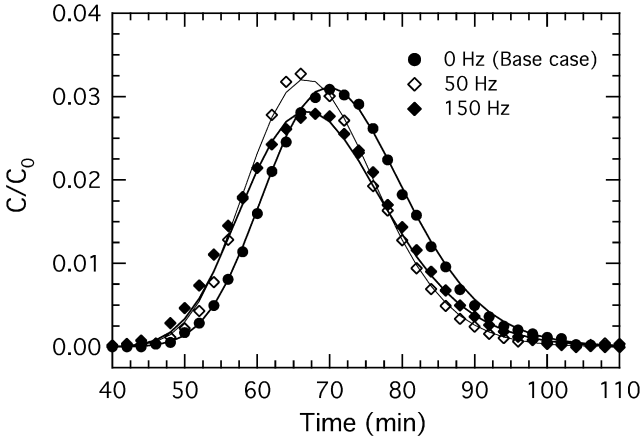

Fig. 3. Breakthrough data (symbols) and fitted analytical solutions (solid lines) for blue microspheres in the absence of acoustic waves (base case, solid circles) and in the presence of acoustic waves at 50 Hz (open diamonds) and 150 Hz (solid diamonds).

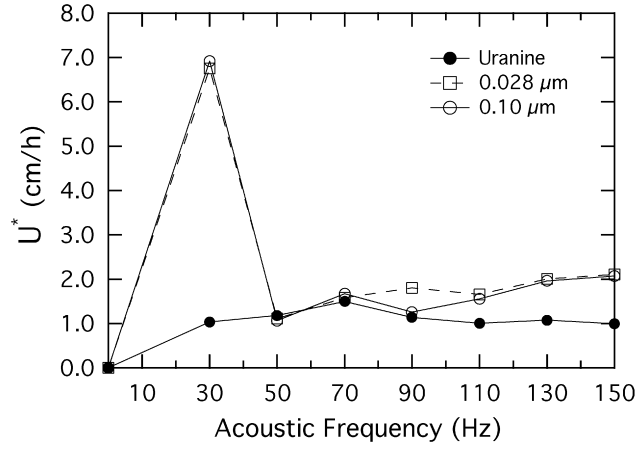

Fig. 4. Experimentally determined component of effective interstitial velocity attributed to acoustics, U^*, at various acoustic wave frequencies for Uranine (solid circle), blue microspheres (open circle), and red microspheres (open square).

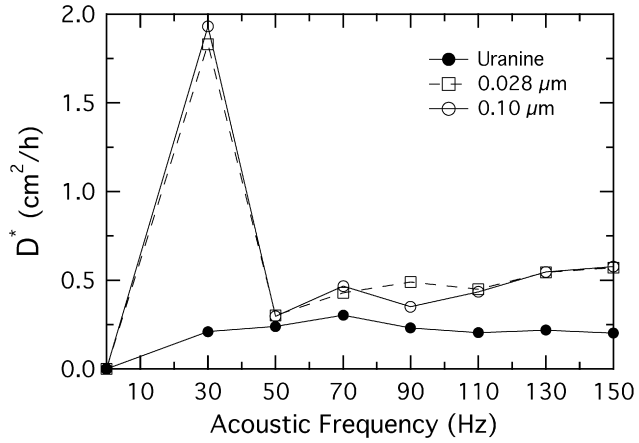

Fig. 5. Component of effective hydrodynamic dispersion coefficient attributed to acoustics, D^*, for various acoustic wave frequencies for Uranine (solid circle), blue microspheres (open circle), and red microspheres (open square).

and red microspheres. For the case of dispersion, the two colloids were affected in a similar fashion by acoustic waves and experienced greater effective dispersion than Uranine. Since U^* and D^* are related by Eq. (3), applied acoustic waves caused an increase in dispersion at all frequencies employed for Uranine and both colloids.

5. Conclusions

The effects of acoustic wave propagation on the transport of colloids in saturated porous media were investigated by injecting Uranine (conservative tracer) as well as blue and red polystyrene microspheres (colloids) into a column packed with glass beads. Experiments were conducted with constant influent acoustic pressure and applied acoustic waves at frequencies ranging from 30 to 150 Hz. An analytical solution to the governing advection–dispersion equation for colloids was obtained through Laplace transform and inverse Laplace transform techniques. A FORTRAN program utilizing the Levenberg-Marquardt nonlinear least squares regression method was written to fit the experimental data to the analytical solution. The results suggested that colloid size did not affect the fitted values of the forward and reverse attachment rate coefficients. The acoustic pressure forcing caused an increase in effective interstitial velocity and dispersion at all frequencies for the conservative tracer and the two colloids, with maximum increase at 30 Hz. This enhanced transport and dispersion is consistent with results obtained for non-aqueous phase liquids in the presence of acoustic waves [24,26–28]. In conjunction with colloid-facilitated contaminant transport during conventional pump-and-treat applications, this may lead to reduced aquifer remediation times. Clearly, the presence of acoustic pressure increases the rate of colloid transport and dispersion in saturated porous media.

Acknowledgments

This work was funded in part by the USA National Science Foundation under NSF Award No. BES-0329398, the Hellenic Republic Ministry of Development: General Secretariat for Research & Development under Award No. 05NON-EU-120, and by the EU research grant INTEREG IIIA Greece–Italy 2000–2006. The content of this manuscript does not necessarily reflect the views of the agencies and no official endorsement should be inferred.

Appendix A. Nomenclature

A	cross-sectional area of column [L^2]
$\mathcal{A}$	defined in (7)
$\mathcal{B}$	defined in (8)
C	concentration of colloids in suspension [M/L^3]
C^*	mass of colloids adsorbed to porous media [M/M]
D	hydrodynamic dispersion coefficient [L^2/t]
D_e	effective hydrodynamic dispersion coefficient [L^2/t]
D^*	component of dispersion attributed to acoustics [L^2/t]
$\mathcal{D}$	molecular diffusion coefficient [L^2/t]
$\mathcal{D}_e$	effective molecular diffusion coefficient [L^2/t]
$\mathcal{H}$	defined in (9)
J_1	Bessel function of order one [–]
M_0	mass injected over cross-section of column [M/L^2]
M_b	mass of glass beads in column [M]
M_I	mass injected [M]
q	seepage velocity [L/t]
Q	volumetric flow rate [L^3/t]
r_1	forward attachment rate coefficient [t^{-1}]
r_2	reverse attachment rate coefficient [$M/L^3/t$]
t	time [t]
U	average interstitial fluid velocity [L/t]
U_e	effective interstitial fluid velocity [L/t]
U^*	component of velocity attributed to acoustics [L/t]
V_b	volume of beads [L^3]
V_t	total inner volume of column [L^3]
V_v	volume of void space [L^3]
x	longitudinal spatial coordinate [L]

Greek letters

α_L	longitudinal dispersivity [L]
δ	Dirac delta function [t^{-1}]
ζ	dummy integration variable
θ	porosity (void volume/total volume) [L^3/L^3]
λ	inactivation constant of suspended colloids [t^{-1}]
λ^*	inactivation constant of adsorbed colloids [t^{-1}]
ρ	bulk density of the solid matrix [M/L^3]
τ	dummy integration variable
τ^*	tortuosity [–]

References

[1] A. Gross, A. Besov, D.D. Reck, S. Sorek, G. Ben-Dor, A. Britan, E. Palchikov, Environ. Sci. Technol. 37 (2003) 4481–4486.
[2] C.V. Chrysikopoulos, P. Hsuan, M.M. Fyrillas, Water Resour. Res. 38 (3) (2002) 1–8.
[3] W.M.J. Bao, E.T. Vogler, C.V. Chrysikopoulos, Environ. Geol. 43 (8) (2003) 968–977.
[4] N. Tien, S. Li, Nucl. Technol. 140 (2002) 83–93.

[5] C.V. Chrysikopoulos, Y. Sim, J. Hydrol. 185 (1996) 199–219.
[6] J.J.W. Higgo, G.M. Williams, I. Harrison, P. Warwick, M.P. Gardiner, G. Longworh, Colloids Surf. A Physicochem. Eng. Aspects 73 (1993) 179–200.
[7] W. Stumm, Colloids Surf. A Physicochem. Eng. Aspects 73 (1993) 1–18.
[8] C.V. Chrysikopoulos, A. Abdel-Salam, Colloids Surf. A Physicochem. Eng. Aspects 121 (1997) 189–202.
[9] R. Kretzschmar, H. Sticher, Phys. Chem. Earth 23 (2) (1998) 133–139.
[10] M.E. Tatalovich, K.Y. Lee, C.V. Chrysikopoulos, Trans. Porous Media 38 (2000) 93–115.
[11] D.R. Champ, J. Schroeter, Water Sci. Technol. 20 (1988) 81–87.
[12] C.G. Enfield, G. Bengtsson, R. Lindqvist, Environ. Sci. Technol. 23 (1989) 1278–1286.
[13] S. Niehren, W. Kinzelbach, J. Contam. Hydrol. 35 (1998) 249–259.
[14] A.A. Keller, S. Sirivithayapakorn, C.V. Chrysikopoulos, Water Resour. Res. 40 (8) (2004) W08304, doi:10.1029/2003WR002676.
[15] W. Um, C. Papelis, Environ. Geol. 43 (2002) 209–218.
[16] A. Abdel-Salam, C.V. Chrysikopoulos, J. Hydrol. 165 (1995) 261–281.
[17] P.W. Reimus, B.A. Robinson, H.E. Nuttall, R. Kale, Mater. Res. Soc. Symp. Proc. 353 (1995) 363–370.
[18] S.C. James, C.V. Chrysikopoulos, J. Colloid Interface Sci. 263 (2003) 288–295.
[19] W.B. Mill, S. Liu, F.K. Fong, Ground Water 29 (1991) 199–208.
[20] J.F. McCarthy, Phys. Chem. Earth 23 (1998) 171–178.
[21] E.T. Vogler, C.V. Chrysikopoulos, Stochast. Environ. Res. Risk Assess. 15 (2001) 33–46.
[22] M.A. Biot, J. Appl. Phys. 28 (2) (1956a) 33–46.
[23] M.A. Biot, J. Appl. Phys. 28 (2) (1956b) 33–46.
[24] I.A. Beresnev, P.A. Johnson, Geophysics 59 (1994) 1000–1017.
[25] E.T. Vogler, C.V. Chrysikopoulos, Geophys. Res. Lett. 29 (15) (2002) 1–4.
[26] E.T. Vogler, C.V. Chrysikopoulos, AIChE J. 50 (12) (2004) 3271–3280.
[27] C.V. Chrysikopoulos, E.T. Vogler, Environ. Sci. Technol. 38 (2004) 2940–2945.
[28] C.V. Chrysikopoulos, E.T. Vogler, Trans. Porous Media 64 (2006) 103–121.
[29] A.M. Thomas, R. Narayanan, Int. J. Heat Mass Transfer 45 (2002) 4057–4062.
[30] A.J. Valocchi, Water Resour. Res. 25 (2) (1989) 273–279.
[31] C.V. Chrysikopoulos, P.K. Kitanidis, P.V. Roberts, Water Resour. Res. 26 (3) (1990) 437–446.
[32] C.V. Chrysikopoulos, P.K. Kitanidis, P.V. Roberts, Trans. Porous Media 7 (2) (1992) 163–185.
[33] Z.J. Kabala, G. Sposito, Water Resour. Res. 27 (3) (1991) 341–350.
[34] C.V. Chrysikopoulos, J. Hydrol. 170 (1995) 181–198.
[35] Y. Sim, C.V. Chrysikopoulos, Water Resour. Res. 31 (5) (1995) 1429–1437; Correction, Water Resour. Res. 32 (5) (1996) 1473.
[36] L. Lapidus, N.R. Amundson, J. Phys. Chem. 56 (1952) 984–988.
[37] Y. Sim, C.V. Chrysikopoulos, Trans. Porous Media 30 (1998) 87–112.
[38] Y. Sim, C.V. Chrysikopoulos, Adv. Water Resour. 22 (5) (1999) 507–519.
[39] P. Weronski, J.Y. Walz, M. Elimelech, J. Colloid Interface Sci. 262 (2003) 372–383.
[40] W.H. Press, S.A. Teukolsky, W.T. Vetterling, B.P. Flannery, Numerical Recipes in Fortran 77: The Art of Scientific Computing, Cambridge Univ. Press, New York, 1992, p. 931.
[41] IMSL, IMSL MATH/LIBRARY User's Manual, Version 2.0, Visual Numerics, Houston, 1991.